PAPER

Check for updates

Predicting glass transition temperature and melting point of organic compounds *via* machine learning and molecular embeddings†

Tommaso Galeazzo [ID] * and Manabu Shiraiwa [ID] *

Gas-particle partitioning of secondary organic aerosols is impacted by particle phase state and viscosity, which can be inferred from the glass transition temperature (T_g) of the constituting organic compounds. Several parametrizations were developed to predict T_g of organic compounds based on molecular properties and elemental composition, but they are subject to relatively large uncertainties as they do not account for molecular structure and functionality. Here we develop a new T_g prediction method powered by machine learning and "molecular embeddings", which are unique numerical representations of chemical compounds that retain information on their structure, inter atomic connectivity and functionality. We have trained multiple state-of-the-art machine learning models on databases of experimental T_g of organic compounds and their corresponding molecular embeddings. The best prediction model is the tgBoost model built with an Extreme Gradient Boosting (XGBoost) regressor trained *via* a nested cross-validation method, reproducing experimental data very well with a mean absolute error of 18.3 K. It can also quantify the influence of number and location of functional groups on the T_g of organic molecules, while accounting for atom connectivity and predicting different T_g for compositional isomers. The tgBoost model suggests the following trend for sensitivity of T_g to functional group addition: $-COOH$ (carboxylic acid) > $-C(=O)OR$ (ester) $\approx$ $-OH$ (alcohol) > $-C(=O)R$ (ketone) $\approx$ $-COR$ (ether) $\approx$ $-C(=O)H$ (aldehyde). We also developed a model to predict the melting point (T_m) of organic compounds by training a deep neural network on a large dataset of experimental T_m. The model performs reasonably well against the available dataset with a mean absolute error of 31.0 K. These new machine learning powered models can be applied to field and laboratory measurements as well as atmospheric aerosol models to predict the T_g and T_m of SOA compounds for evaluation of the phase state and viscosity of SOA.

Environmental significance

Secondary organic aerosols (SOA) represent a major component of atmospheric particulate matter and their accurate representation in aerosol models is a demanding problem in atmospheric chemistry. SOA partitioning is impacted by the particle phase state, viscosity and glass transition temperature (T_g) of organic compounds. Here, we develop a machine learning model to predict glass transition temperature of organic compounds. The new model considers molecular structure, functionality and atomic interconnectivity, discerning compositional isomers. It reproduces experimental measurements very well, out-performing previous compositional parametrizations. This powerful tool offers state-of-the-art performances and its implementation in aerosol models would contribute to a better evaluation of SOA effects on climate and air quality.

1. Introduction

Secondary organic aerosols (SOA) are major components of particulate matter in the atmosphere, influencing climate, air quality, and public health.[1,2] SOA formation and evolution are complex processes, which have been the subjects of extensive investigations with field observations, laboratory experiments, and modeling.[3,4] Aerosol models are useful computational tools which can simulate the formation and evolution of SOA chemical composition and properties. The development of SOA models represents one of the most demanding and challenging problems in atmospheric chemistry.[5] These models rely on accurate representation of physical properties including particle viscosity and bulk diffusivity that influence gas-particle partitioning of semi-volatile and low volatility organic compounds.[6]

Department of Chemistry, University of California, Irvine, CA92697, USA. E-mail: tommaso.galeazzo@gmail.com; m.shiraiwa@uci.edu

† Electronic supplementary information (ESI) available. See https://doi.org/10.1039/d1ea00090j

SOA viscosity can be estimated using the glass transition temperature (T_g) of the constituting organic compounds.[7–9] While there is a fair amount of measured T_g of organic compounds,[7] there are only limited number of T_g measurements for SOA compounds.[10–12] To fill such measurement gaps, various T_g parametrizations have been developed based on molecular properties including molar mass and atomic oxygen to carbon ratio,[13] saturation mass concentration,[12,14,15] and elemental composition (*e.g.*, number of C, H, N, O, S atoms).[8,15] Moreover, Rothfuss and Petters[16] have introduced an empirical group contribution estimation based on functional groups presence within a molecule. Their results suggest functionalization is a crucial predictive parameter for molecular T_g. These parameterizations are simple, practical, and versatile prediction methods, which have been applied to estimate SOA viscosity for high-resolution mass spectrometry[8,17–19] and also implemented into thermodynamic,[20,21] gas-phase chemistry models[9] and chemical transport models.[5,22,23] These parameterizations, however, have relatively larger uncertainties ($\sim$25 K) and they do not account for molecular structure and functional groups presence. Notably, Rothfuss and Petters[16] found that viscosity of weakly functionalized organic compounds is highly sensitive to functional groups addition and location within a molecule. Thus, there is a strong need to discern between compositional isomers and to account explicitly for functionality and molecular structure.

In cheminformatics molecular descriptors are mathematical objects representing chemical species at different levels of complexity, covering from 0-D atomic information to 3-D molecular structures.[24] They are commonly used in medicinal chemistry to develop models predicting chemical activities (Quantitative Structure–Activity Relationship, QSAR) or physical properties (Quantitative Structure–Property Relationship, QSPR) of pure compounds in absorption, distribution, metabolism, excretion and toxicity (ADMET) studies.[25] Over the years there have been studies focusing on the prediction of the melting point (T_m) of an organic compound *via* QSPR models: it is a task of particular interest because of the correlation of the T_m with the vapor pressure, boiling point, glass transition temperature, and water solubility.[26–28] In environmental sciences, the MPBPWIN module from the EPI Suite software by the Environmental Protection Agency (EPA) is the standard reference for the estimation of the T_m of environmentally-relevant organic compounds.[29] This QSPR model is built on a simple group-contribution-method where a vectorized list of functional groups acts as the molecular descriptor of a species. The EPI Suite performs well for predicting the T_m of small molecules with a few functional groups, but it overestimates T_m of more structurally complex and aromatic compounds.[29] Therefore, the need for a powerful estimation model that could be more accurate in its prediction and in capturing molecular complexity. However, developing an accurate T_m model is challenging due to the quality of the available datasets and the variability of the used molecular descriptors which induce large errors and uncertainty in model generalizability (*i.e.*, accurate error estimation when analyzing new molecules).

Over the last years, developments in artificial intelligence and machine learning (ML) have overspilled to cheminformatics. Notably, text analysis techniques borrowed from Natural Language Processing (NLP) have been used to learn chemically contextualized molecular descriptors from canonical molecular representations including SMILES (Simplified Molecular Input Line Entry System: molecular strings notations to describe unique chemical structures). Jastrzębski *et al.*[30] showed that SMILES can be used to learn contextualized chemical descriptors of molecules *via* convolutional neural networks (CNN). Recently, Gómez-Bombarelli *et al.*[31] developed a chemical Variational Auto Encoder (VAE): a generative model based on a Recurrent Neural Network (RNN) that learns compressed numerical representations from SMILES (encoding step) and generates molecules with target properties from the chemical space (generative step). Segler *et al.*[32] showed that SMILES can be used to generate bioactive molecular candidates from small datasets using RNNs and by transferring the learned molecular descriptors and knowledge to large datasets. Jaeger *et al.*[33] developed mol2vec, an algorithm that learns molecular descriptors as high dimensional embeddings of molecular substructures (*i.e.* "molecular embeddings") from SMILES notations by combining the word2vec and Morgan algorithms.

Recently, a few studies have explored the performances of different combinations of ML models and molecular descriptors in predicting the T_m of organic compounds.[34–36] The resulting models largely outperform the EPI Suite in predicting T_m, suggesting an increasing ability of ML models and complex molecular descriptors in predicting T_m of pure compounds and potentially their T_g. These studies have focused on the development of molecular descriptors from molecular graphs *via* convolutional embedding methods.[60,61] The developed embeddings (*i.e.*, convolutional embeddings) reach extremely high prediction accuracies, but they can result in significant drawbacks with regards to model deployment and portability. In these approaches both the embedding and the property prediction steps are engrained in the Convolutional Neural Network (CNN). The major caveat of using the former approach is that the dataset and CNN architecture cannot be decoupled, and the embeddings are generated *in situ* from the very specific dataset. Therefore, the resulting convolutional embeddings are dataset specific and cannot be loaded and used for other tasks. Moreover, in such approaches the development of the target QSAR model requires the optimization and training of the CNN, which are very computationally demanding tasks. As a consequence, these models lack portability, transferability and scalability due to the *in situ* generation of molecular descriptors dependent on the dataset of origin, and the absence of a finalized trained model which could be transferred to other datasets. On the other hand, mol2vec reaches state-of-the-art performances to statistically infer various molecular properties in supervised learning tasks by generating unique high-dimensional vectors from a pretrained embedding model. As a result, it can be easily transferred and included in the analysis of complex chemical systems with large numbers of diverse compounds.

© 2022 The Author(s). Published by the Royal Society of Chemistry

Environ. Sci.: Atmos., 2022, **2**, 362–374 | **363**

Here we introduce the first ML-driven T_g prediction method based on molecular embeddings. We use different machine learning algorithms to predict T_g by explicitly considering molecular structure, functionality and atomic interconnectivity, outperforming previous T_g parameterizations. The new model can reproduce experimental T_g data and the influence of number and location of functional groups within the molecule on T_g. We extend the investigation to the prediction of T_m using a large experimental dataset with ~200 000 compounds. We develop a new model for T_m prediction, reaching close to state-of-the-art performances. These new ML powered T_g and T_m models can be exploited to predict viscosity in aerosol models involving organic molecules, with future applications that go beyond aerosol chemistry and extend to modeling of organic mixtures.

2. Methods

2.1 Datasets and preprocessing

We have compiled available datasets of T_g and T_m for organic compounds with SMILES strings. The datasets are cleaned using RDKit, a publicly available python library for cheminformatics tasks.[37] Data cleaning is composed by three different steps: filtering of molecules that cannot be recognized by RDKit, conversion of SMILES strings to their canonical form, and averaging over the target property for compounds that have multiple entries with different T_g or T_m values. We have performed initial screening to delete most of the heavier compounds from the datasets (MW > 600) and to include only compounds with H, C, O, N, S, F, Cl, and Br atoms.

The largest measurement dataset reporting T_g of organic compounds (T_g-Measured) contains 394 measurements.[7] The original dataset has been enriched with recently measured T_g for 7 atmospheric compounds[12] and with theoretically-derived T_g for 9 linear alkanes from molecular dynamics simulations.[38] The T_g-Measured dataset is composed of 415 entries and after the cleaning step it comprises 298 unique entries. Due to the scarcity of available experimental T_g data, we train separate T_m models using larger datasets of experimental T_m. T_g can be estimated from T_m using the structure–activity relationship known as the Boyer-Kauzmann rule: $T_g = g \times T_m$ with g as a constant to be 0.7 based on analysis by Koop *et al.*[7] The first experimental T_m dataset is formed by values extracted from patents by Tetko *et al.*[39] (T_m-Tetko), while the second dataset is the "Bradley good T_m dataset" (T_m-Bradley),[40] a highly curated experimental T_m dataset of drug-like small molecules. The T_m-Tetko dataset is the largest publicly available T_m dataset: it contains 228 174 entries and it accounts for 220 348 species after cleaning.

The final step of dataset preprocessing is the conversion of canonical SMILES into molecular embeddings. We have used the mol2vec library to generate unique 300-dimensional embeddings (*i.e.*, "molecular embedding") for each chemical species in the different datasets (Table 1).

2.2 Model selection and training

2.2.1 Measured T_g dataset. We apply two different algorithms, Random Forest (RF) and Extreme Gradient Boosting

Method (XGBoost), to develop T_g regressor models based on the T_g-Measured dataset. We focused our investigations on Gradient Boosting Method (GBM) algorithms due to the relatively easy training process, and their high rate of success in both regression and classification tasks in QSAR/QSPR studies.[33,34] Notably, XGBoost is a recent gradient bosting implementation developed by Chen and Guestrin (2016)[41] with important improvements over previous GBM algorithms. It is designed to be both computationally efficient (*e.g.*, fast to execute), highly accurate and powerful. The XGboost algorithm has been gaining large traction in the ML community due to its effectiveness in developing robust classification and regression models. The performance metrics employed to evaluate the regression tasks include mean absolute error (MAE), mean squared error (MSE), and coefficient of determination (R_{CV}^2).

Model selection and optimization are conducted *via* a nested cross-validation (also known as "double cross-validation"). This model development technique allows to estimate an almost unbiased and low variance true error when data are scarce.[42–44] A previous study has shown that a nested cross-validation is particularly suitable for QSAR/QSPR model development and when datasets are small (*i.e.* <1000 entries).[43] Fig. 1a shows a simplified representation of the 10-fold nested cross-validation implemented for the training of T_g models with the T_g-Measured dataset. The model development task is structured as a double loop composed by an outer loop for model evaluation (*i.e.*, outer K-loop) and an inner loop for model selection and optimization (*i.e.*, inner J-loop).[44] Initially, the entire dataset is divided into K folds ($K = 10$ in this study): K-1 folds are used to train the model on the best set of hyperparameters and one fold is kept aside to evaluate the error of the trained model on unseen data for model evaluation. At each i iteration of the outer loop ($1 < i < K$), the ith fold used for model training (*i.e.*, K_i) is passed to the inner J-loop for model optimization *via* hyperparameters selection. To carry the optimization of the model, K_i is further divided into J sub-folds with $J = 10$ in this study.

During this step, J-1 sub-folds are used to select the best hyperparameters (*i.e.*, *hyperparameters tuning* based on the specific model architecture) and the remaining J sub-fold is a validation set used to evaluate the performance of the model developed with this specific parameter combination. The process is repeated for J times on the different J-folds combinations obtained from further split of K_i. The model optimization step is repeated for each K-fold of the outer loop, resulting in K different models developed from the K data combinations. As a result, for each model architecture (*e.g.*, RF, XGBoost) we have conducted $n \times 10 \times 10$ fits and error estimations, where n is the total number of single values that can be assumed by individual model architecture parameters. Once we have identified the best model parameters, we have trained the model on the whole dataset and used the estimated errors from the outer cross-validation as the final true value of MAE. This approach enables to reach the best trade-off between bias and variance by selecting the best model parameters, while obtaining a true error estimation by accounting for a vast number of possible data combinations and cross-validation. The RF regressor model is implemented in Python using scikit-learn, a library for

Table 1 A summary of the datasets used to develop the T_g and T_m prediction models

Data	Dataset name	Literature	Initial entries	Final entries
T_g, experimental	T_g-Measured	Koop *et al.* (2011)[7] Zhang *et al.* (2019)[12] Martín-Betancourt *et al.* (2009)[38]	415	298
T_m, experimental	T_m-Tetko	Tetko *et al.*, (2016)[39]	228 174	220 348

scientific computing and machine learning.[45] The XGBoost regressor model is implemented *via* xgboost, a Python library for optimized distributed gradient boosting model development.[41] The hyperparameters of our regressor models were selected through a grid search approach: we selected a range of plausible values for each hyperparameter (*e.g.*, estimators, maximum depth of trees, learning rate, *etc.*) and we have trained as many models as the possible combinations of available hyperparameters. Finally, we selected the best T_g regression model whose combination of hyperparameters provided the lowest error in the nested cross-validation step. The best T_g regression model (tgBoost) developed *via* a XGBoost regressor
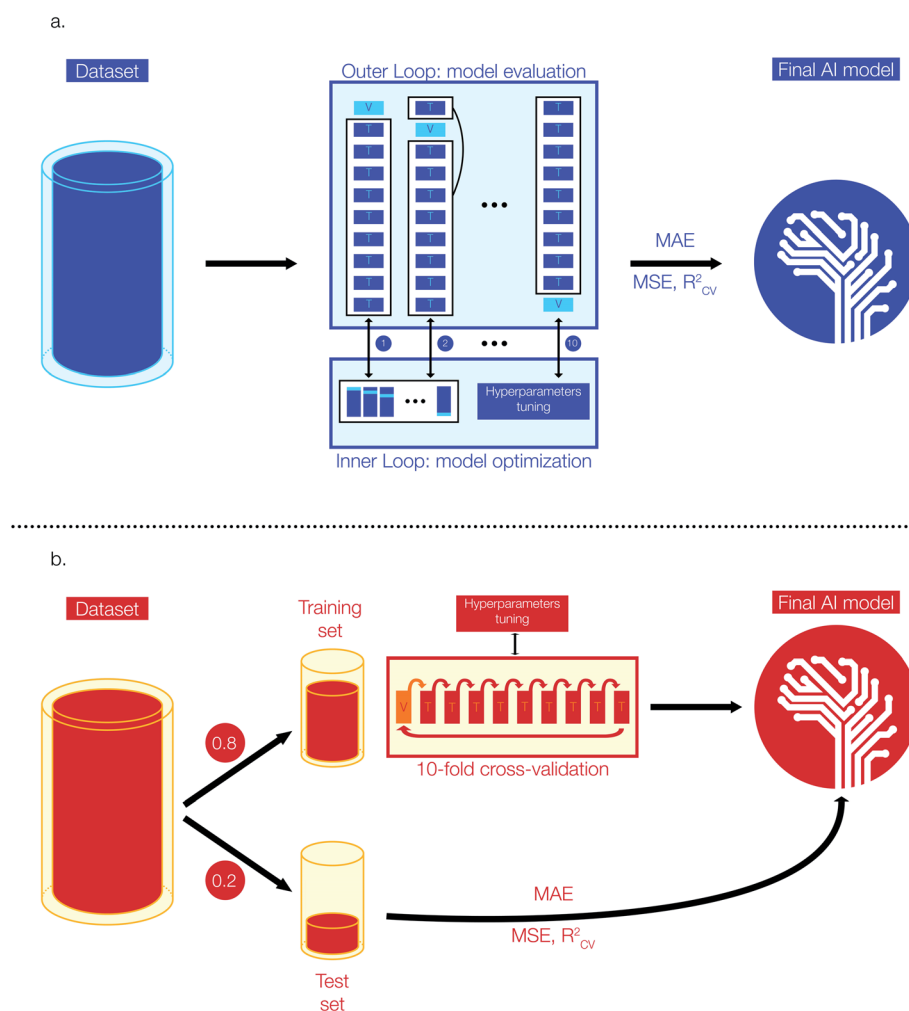

Fig. 1 Schematic representation of the approaches used to develop (a) the T_g regression model based on the T_g-Measured dataset, and (b) the T_m regression models based on the T_m-Tetko, and the T_m-Bradley datasets. The top scheme is used to develop a Nested-cross validation based model: each block in the outer-loop box illustrate K_i, the data combination from the i iteration ($1 < i < 10$); the double-headed arrows and corresponding numbers show how at each ith iteration the K_i is passed to the inner J-loop for model optimization and how the tuned i model is passed back for model evaluation after the selection of the best hyperparameters; the MAE, MSE, R_{CV}^2 are estimated using the average values outputted from the outer loop models. The lower scheme illustrates the simple cross-validation approach: the input data are divided into a training (80% of total input data) and test (20% of total input) set. The training set is divided into K-folds ($K = 10$) and for each i iteration ($1 < i < 10$) the best hyperparameters are evaluated for the different K_i folds combination. The model with the lowest error is selected as the final AI model and the MAE, MSE, R_{CV}^2 are measured on the unseen data from the test set.

© 2022 The Author(s). Published by the Royal Society of Chemistry

Environ. Sci.: Atmos., 2022, **2**, 362–374 | **365**

and through the nested cross-validation is composed by: 100 estimators, a maximum depth of 9 trees, a learning rate of 0.1, and a γ equal to 30.

2.2.2 T_m-Tetko, T_m-Bradley and T_m-EPI datasets. Based on the large size of the dataset (*i.e.* ~220 000) we built the T_m regression models using Deep Neural Network (DNN) and XGBoost architectures.[33–35] The performance metrics employed to evaluate these regression models are MAE, MSE, and R_{CV}^2 similarly to the development of the T_g model. All the T_m datasets are composed by enough entries to allow model validation *via* a simple 10-fold cross-validation approach.[46] Fig. 1b shows a simplified representation of the stages implemented to develop the T_m models. Initially, the preprocessed data have been divided into a training and test set respectively composed by 80 and 20% of the input data. The test set is kept aside during model development and used to evaluate the performances of the models on unseen data. The training sets have been further divided into 10 folds and model parameters have been selected (*i.e.*, hyperparameters tuning) using iteratively 9 folds for training and one fold for validation. Similar to the process used to select the best regressor model for T_g, we have used a grid search approach to select the best hyperparameters for developing the T_m regression. We selected a range of plausible values for each hyperparameter (*e.g.*, number of nodes in the activation layer, number of hidden layers, optimizer, number of nodes in hidden layers, activation functions, dropout, learning rate, *etc.*) and we have trained as many models as the possible combinations of available hyperparameters. The parameters for the best T_m model are the ones reporting the lowest average error on the 10-fold cross-validation step. The DNN models have been implemented using Keras, a Python machine learning library for deep learning and based on Theano.[47] The best DNN model was obtained using the T_m-Tetko dataset, and its detailed architecture is: 1 input layer with 300 nodes, 3 hidden layers with 32 nodes each, ReLU activation functions for the hidden layers followed by a linear activation function on the single node of the output layer, an Adam optimizer added to the loss function, mini-batches of 32 datapoints during training, a learning rate of 0.001, 100 epochs of training and no dropout.

3. Results

3.1 T_g regression model performance

Table 2 shows the performances of our T_g models trained on the T_g-Measured dataset by using molecular embeddings from mol2vec as molecular descriptors. The results are compared to our previous compositional parametrizations based on elemental composition where the input variables are the number of C, O, H, N and S atoms of species: the equations on which the compositional parametrizations are implemented are logarithmic ordinary least squared (OLS) regressions.[8,15] All the models developed in this study using ensemble method algorithms (RF, XGBoost) perform better than the compositional parametrizations. The RF regression model has an estimated MAE of 22.2 K. The best results are achieved by the XGBoost algorithm, which performs remarkably well in predicting the T_g of compounds from the T_g-Measured dataset, as shown in the

Table 2 Comparison of the regression tasks on T_g and T_m datasets from this work with results from previous studies

Dataset	Algorithm[a]	MAE (K)	RMSE	R_{CV}^2	R	Study
T_g-Measured	RF	22.2	26.9	0.86	0.94	This work
	XGBoost	18.3	15.3	0.99	0.99	This work
	OLS	27.2		0.83	0.91	8 and 15
T_m-Tetko	DNN	31.0	40.1	0.6	0.77	This work
T_m-Bradley	CNN	26.2	35.5			35[b]
	Baseline	43.3	57.7			35[b]
	ASNN		32.0			34[b]
	GCNN	28.85		0.78		36[b]
	RF	34.62		0.66		36[b]
	GPR	29.41		0.75		36[b]

[a] RF = random forest, XGBoost = extreme gradient boosting method, OLS = ordinary least squares (*i.e.*, compositional parametrizations[8,15]), DNN = deep neural network, CNN = convolutional neural network, GCNN = graph convolutional neural network, ASNN = adversarial neural network, GPR = Gaussian process regression. [b] The datasets used in these studies are all different variations of the "Bradley Good Melting Points Dataset" from Bradley *et al.*[40]

correlation plot in Fig. 2, with $R = 0.99$ and $R_{CV}^2 = 0.99$ with no significant outliers. The MAE of the single best tgBoost model developed on the whole T_g-Measured dataset is 3 K, which represents a dramatic improvement compared to the compositional parametrizations with MAE of 27.2 K. Note, however, that the true cross-validation MAE of the tgBoost model on unseen data is 18.3 K as measured on the validation sets of the outer loop 10-fold cross-validation. This is the true error which is statistically inferred by the outer validation loop of the nested cross-validation, and which should be considered for model predictions on molecules outside of the T_g-Measured dataset.
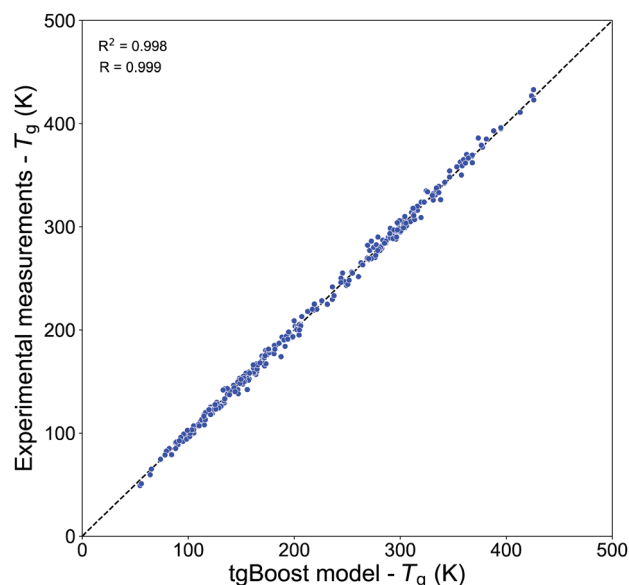

Fig. 2 Correlation plot between the predicted T_g values by the tgBoost model and the experimental T_g values from the T_g-Measured dataset.

3.2 T_g model evaluation

To evaluate if the tgBoost model has learnt to recognize the relationship between molecular properties/structure and T_g, we assess the performance of the tgBoost model by simulating T_g in relation to the molecular structure and the presence of functional groups within a molecule, along with comparison with reported values and the T_g compositional parameterization. Fig. 3 shows the predicted T_g for the linear n-alkane series (n = 2–20) modeled *via* the tgBoost model and the T_g compositional parametrization.[8] The results are compared to the simulated values for n-alkanes (n = 2–10) by molecular dynamics (MD) simulations,[38] which were validated against measurements and included in the training dataset. The tgBoost model shows an excellent agreement with MD values, reproducing a smooth increase of T_g. Compared to the tgBoost model, the compositional parametrization underestimates T_g for n < 8, while overestimating for n > 13, as the T_g predicted by the parametrization follow a logarithmic growth (*i.e.*, ingrained in the original equation) proportional to the number of C atoms added to the alkane chain.

Remarkably, the tgBoost model repeats a smooth increase of T_g for n > 11 after a dip between n = 10–11. MD simulations suggest that the slower T_g increase is a non-linear phenomenon resulting from the combination of structural inner- and intermolecular effects occurring in the bulk phase of pure n-alkanes.[38] It is possible to assume that the higher degree of available conformational rearrangements of longer n-alkanes would lead to a lower T_g with each addition of a C atom to the alkyl chain. However, MD simulations suggest that longer n-alkanes can be easily trapped in pipe cages within the bulk phase of the glassy material and be prevented from rearranging in stable conformations that would lead to crystallization. With each addition of a C atom to the alkyl chain the interplay

between these contrasting effects would need to be taken into account for T_g evaluation. As the MD values were included in the training dataset for the tgBoost model, it is possible that the tgBoost model might have extrapolated the trend observed for the lower mass molecules (*i.e.*, n < 10) and expanded it to n > 11 based on the similarity between molecular embeddings of n-alkanes. To validate and resolve this issue, T_g measurements or MD simulations for higher n-alkanes are necessary. This result confirms the high performance of ML driven molecular descriptors (*i.e.*, information rich embeddings) in capturing subtle variations in experimental/simulated data in relation to changes in the molecular structures and non-linear combinatorial physical effects.

Fig. 4 compares the experimental T_g measurements of n-alkyl alcohols (n = 1–16) with the respective T_g values predicted by the tgBoost model and the compositional parametrization.[8] Primary, secondary and tertiary alcohols are all isomers with same elemental composition and consequently the compositional parametrization predicts the same values for all species, representing its major limitation. Overall, the compositional parametrization tends to overestimate the T_g of primary alcohols and to underestimate for secondary alcohols. In contrast, the tgBoost model predicts T_g in consistence with measurements, showing lower T_g for primary alcohols and higher T_g for secondary and tertiary alcohols when n < 7. This behavior is consistent with the results by Rothfuss and Petters,[16] who highlighted that smaller T_g values are typically observed for primary alcohols whereas longer chain alcohols with branching and midchain –OH group have larger T_g values. The values
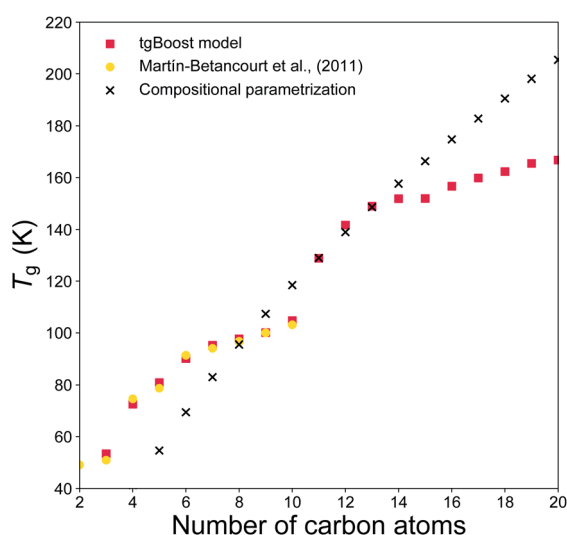
Fig. 3 T_g values predicted for the n-alkanes (n = 2–20) by the developed tgBoost model (red dots), molecular dynamics simulations (yellow squares),[38] the T_g compositional parametrizations (black crosses).[8]
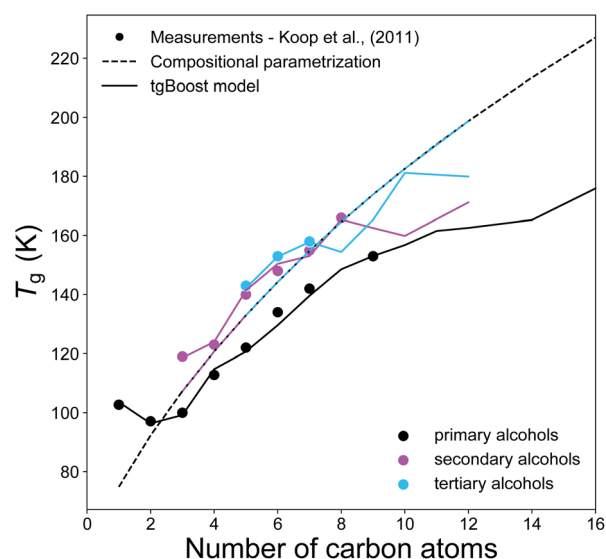
Fig. 4 T_g values of primary alcohols (black), secondary alcohols (magenta), and tertiary alcohols (light blue) as a function of the number of carbons of the n-alkyl chain. The markers represent the available experimental measurements,[7] the solid lines represent the predicted values by the tgBoost model, and the dashed lines represent the T_g predictions by the compositional parametrization.[8] Note that primary alcohols have a terminal –OH group, and secondary and tertiary alcohols have one –OH group placed on the second and third carbon atoms of the alkyl chain, respectively.

© 2022 The Author(s). Published by the Royal Society of Chemistry

Environ. Sci.: Atmos., 2022, **2**, 362–374 | **367**

modeled by tgBoost for secondary and tertiary alcohols overlap at this stage. It is hard to refine the tgBoost model performance for this task due to the lack of sufficient experimental measurements for tertiary alcohols. However, our results indicate that molecular embeddings would be able to capture oscillations in T_g due to small variations in molecular structures (such as the displacement of the –OH group along the alkyl chain) if more data were included during model training.

Fig. 5 shows the experimental and modeled T_g of n-alkanes, monoalcohols, diols and triols. Note that, monoalcohols have the –OH group attached at the end of their alkyl chain, diols have the two –OH groups attached at the two opposite ends of their alkyl chain, and triols have the same structure of diols with an additional –OH group attached to the second carbon of their alkyl chain counted from one of its ends. The measurements are compared to the corresponding predictions by the tgBoost model and the compositional parametrization.[8] Both models reproduce an increase in T_g observed with the addition of one to three –OH groups to the alkyl chain. Remarkably, both models reproduce the increase of 30–50 K observed with the addition of each –OH group. These results are in good agreement with a previous study, which reported an almost linear increase in T_g value for the addition of –OH groups to the skeleton of raw alkyl chains.[16] The compositional parametrization exhibits a logarithmic growth upon an increase of n, overestimating in general T_g values of alcohols. These results emphasize the predictive power of molecular embeddings and ML models in aerosol modeling over simple compositional parametrizations, given that atmospheric SOA contain many alcohols.[48–50]

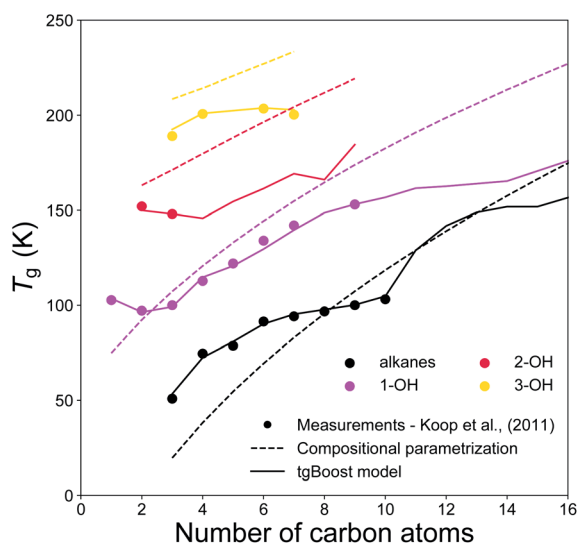

Fig. 5 T_g values of n-alkanes (black), monoalcohols (magenta), diols (red), and triols (yellow) as a function of the number of carbons of the n-alkyl chain. The markers represent experimental measurements,[7] the solid lines represent the predicted values by the tgBoost model, and the dashed lines represent the T_g predictions by the compositional parametrization.[8] Note that mono-alcohols have one terminal –OH group, diols have two –OH groups placed at the extremities of the carbon chain, and triols have a similar structure to diols but with an additional –OH group placed on the second carbon atom of the chain counted from one of the extremities.

These results should motivate future studies to adopt molecular embeddings and machine learning algorithms to develop predictive models of organic molecules. Note that there are limitations to be accounted when using models like tgBoost. As reported in Fig. 4 and 5 the model can discern among compositional isomers of simple mono-alcohols (*i.e.* primary, secondary and tertiary alcohols) and it can simulate the increase in T_g by each –OH addition similarly to the compositional parametrization and the few available experimental data points of diols and triols. However, tgBoost should be used with precautions when working with these compound classes: as there are limited amount of observational data for tertiary alcohols, diols and triols, tgBoost might neglect possible trends in T_g for those molecular classes. Therefore, when possible, it would be good to compare tgBoost predictions with other T_g QSPR models developed on different datasets and physical properties. These limitations underline the importance of collecting more experimental data on T_g of atmospherically-relevant organic molecules.

We have conducted further proof-of-concept investigations on the performance of tgBoost in distinguishing other compositional isomers and on the effects on T_g due to the addition of carboxylic groups to an alkyl chain. Fig. 6 shows the T_g of different compositional isomers as predicted by tgBoost. It illustrates the T_g predictions as a function of the number of carbon atoms of the species in compositional isomers grouped as (a) ethers and alcohols, (b) ketones and aldehydes, and (c) esters and carboxylic acids, with the respective functional groups positioned at the end of the alkyl chain. Our results suggest the following trend for sensitivity of T_g to functional group addition: –COOH (carboxylic acid) > –C(=O)OR (ester) ≈ –OH (alcohol) > –C(=O) (carbonyl) ≈ –COR (ether) where the carbonyl group category comprises –C(=O)R (ketone) and –C(=O)H (aldehyde). Overall, the results are in good agreement with previous viscosity measurements, which suggested the following trend in viscosity sensitivity to functional group addition –COOH (carboxylic acid) ≈ –OH (alcohol) > –ONO$_2$ (nitrate) > –C(=O) (carbonyl) ≈ –C(=O)OR (ester) > –CH$_2$ (methylene).[16] Our results suggest that for weakly functionalized compounds the addition of an ester functional group to the alkyl chain can strongly increase the T_g of a molecule, particularly for smaller compounds with $n < 6$ (see Fig. S4† in ESI). This effect may be due to conformational effects resulting from the addition of an alkoxycarbonyl group, which would induce lower flexibility in the aliphatic component and a lower degree of transformation between *trans*- and *cis*-stereoisomers in the carbon chain. It is expected that ketones and aldehydes have a relatively lower T_g compared to alcohols and carboxylic acids as there are no functional groups that may be involved directly in hydrogen bonds in the bulk phase of pure materials. However, their potential role in increasing the overall T_g of SOA mixtures should be noted since the carbonyl group may still participate in hydrogen bonds in presence of hydrogen donors. Further investigations are needed to assess how the interplay of multiple functional groups can affect T_g of multicomponent complex mixtures.
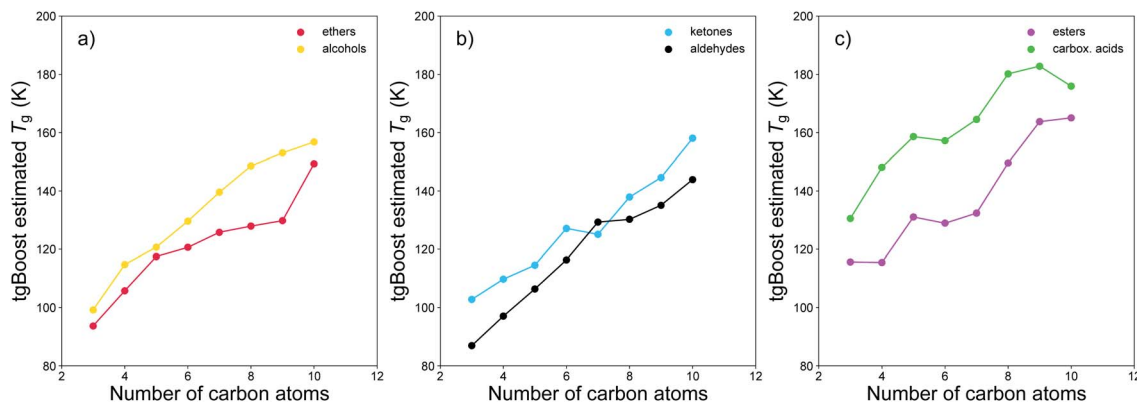
368 | *Environ. Sci.: Atmos.*, 2022, **2**, 362–374

© 2022 The Author(s). Published by the Royal Society of Chemistry

Fig. 6 Estimated T_g of weakly functionalized isomeric molecules by functional group as a function of the number of carbon atom within the molecule. Isomers are grouped as (a) ethers and alcohols, (b) ketones and aldehydes, and (c) esters and carboxylic acids. The respective functional groups are positioned at the end of the alkyl chain for all species.

Carboxylic acids represent a major fraction of SOA[50] and a better representation of carboxylic acids data is particularly relevant for aerosol models. Fig. 7 illustrates the predicted T_g by the tgBoost model and the compositional parametrization[8] for the addition of one to three carboxylic groups to the alkyl chain. Both methods predict increasing T_g values for each addition of a carboxylic group to the molecule. At equal number of C atoms in the molecule, the mean increase in T_g between mono carboxylic and dicarboxylic acids is 63 and 53 K for the tgBoost model and compositional parametrizations, respectively. The tgBoost model shows a steady increase in T_g for mono-carboxylic acids and interestingly it predicts a decline in T_g for dicarboxylic acids with $n > 5$ and no increase in T_g value for tricarboxylic acids. It should be noted that the acidity of dicarboxylic acids lowers with the addition of C atoms to their alkyl

chain due to the electron donating nature of the alkyl group. This decrease is proportional to the addition of new C atoms to the aliphatic chain with the highest reductions observed for the first four carbon additions.[51] The acidity of dicarboxylic acids depends also on the conformation of the species, with *trans*-structural isomers being considerably more acidic than the equivalent *cis*-structural isomers. A lower acidity implies a reluctancy for the molecule to release protons, therefore a more stable structure and a lower strength in hydrogen bonding.[52,53] It has been shown that T_g is strongly influenced by the presence of hydrogen bonds, notably because hydrogen bonds promote the crystallization process that leads to the transition into a solid state.[54] T_g is also strongly affected by stereoisomerism because rotamers and conformers slow down the crystallization process.[55] Similar acidity and the presence of more stereoisomers in di- and tri-carboxylic acids with longer alkyl chains would combine and result in comparable strengths of hydrogen bonds with addition of C atoms to the molecular structure. It is possible that this effect may justify the decreasing or constant predicted T_g of dicarboxylic and tricarboxylic acids upon increasing carbon number.
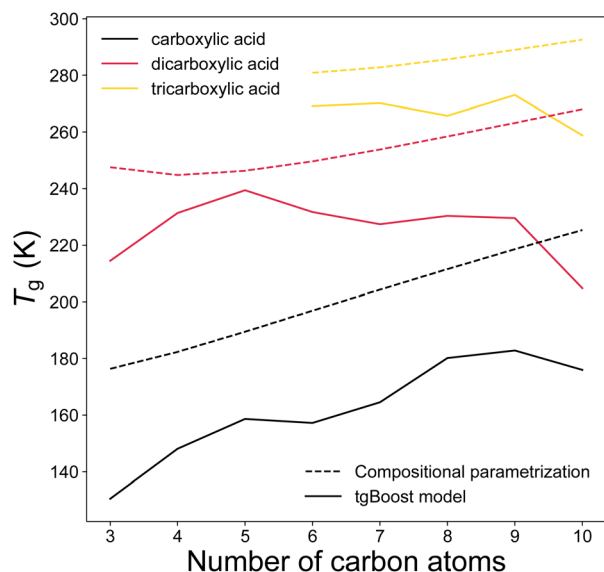
3.3 Domain of application and model comparison

It is fundamental to verify the correct domain of applicability of developed QSAR/QSPR models because potentially any of these models could be used to predict the physical properties of any chemically acceptable molecule. Since our domain pertains to atmospheric chemistry, we test how well the tgBoost model predictions compare to the values from atmospherically-relevant compounds. There are unfortunately no large available datasets reporting experimental T_g values of atmospheric species and the data can only be estimated from the best available T_m models through the Boyer-Kauzman rule where $T_g = g \times T_m$, with $g = 0.70085\ (\pm0.00375)$.[7] Similarly to the approach used to develop the T_g compositional parametrizations,[8,15] we have used a list of SOA compounds compiled by Shiraiwa *et al.*[56] and we have estimated the T_g of these compounds from the computed T_m values by EPI Suite. The

Fig. 7 T_g of linear monocarboxylic, dicarboxylic and tricarboxylic acids as a function of the number of carbon atoms in the alkyl chain as predicted by the tgBoost model (solid lines) and the T_g compositional parametrization (dashed lines).[8]

© 2022 The Author(s). Published by the Royal Society of Chemistry

Environ. Sci.: Atmos., 2022, **2**, 362–374 | **369**

estimated T_g are compared to the T_g predictions from the tgBoost model to assess its application to atmospheric chemistry modeling.

Fig. 8a shows the results of such comparison. Overall, the values predicted using the tgBoost are similar to the ones estimated using the T_m from EPI Suite with MAE = 27.6 K, R = 0.794, and R_{CV}^2 = 0.455. Many datapoints are positioned below the 1 : 1 correlation line, indicating that the tgBoost model tends to underpredict the T_g of SOA compounds compared to EPI Suite. This behavior is consistent with the EPI Suite guideline that reports a tendency for the MPBPWIN module to overestimate the T_m of large and multi-functionalized molecules, such as aromatics and complex carbonyl bearing compounds.[29] The shaded pink square in Fig. 8a highlights a cluster of 20 molecules whose values are overpredicted by a factor of 100–150 K by EPI Suite, and which are all complex multi-functional branched carbonyl compounds with ether and alcohol segments within their molecular structure (see Fig. S2†).

Fig. 8b shows the correlation between the T_g values predicted from the compositional parametrization[8] and those estimated from EPI Suite T_m. In this case the T_g values predicted by the two models are very similar with a very low MAE of 14.6 K, a high positive correlation of R = 0.917, and a relatively low variance of R_{CV}^2 = 0.839. This result suggests that the models have similar prediction capability and the molecular descriptors used to develop the models have similar limitations. Notably, due to the limitations of EPI Suite, the compositional parametrizations may also tend to overestimate T_g of organic species as pointed by the high correlation between the two methods. The shaded orange square highlights a cluster of 30 molecules whose values are overpredicted by a factor of 55–75 K by EPI Suite. The largest divergences are observed for nitrogen bearing large compounds with carbonyl, alkane ring and alcohol segments within their molecular structures (see Fig. S3†).

These results imply that the tgBoost model is applicable to SOA compounds, providing more realistic T_g of organic molecules with complex structure and multiple functional groups

compared to the EPI Suite. Remarkably, we observe that molecular embeddings can overcome the limitations affecting the performances of the EPI Suite and the compositional parametrizations. The tgBoost model performs well in predicting T_g of SOA compounds and it has good potential for applications to the modelling of aerosol chemistry.

3.4 T_m regression model performance

We have also trained multiple ML models on publicly available datasets of T_m with the aim to build a T_m regression model based on large amounts of experimental data to be used for the estimation of T_g using the Boyer-Kauzmann rule. Table 2 shows the performances of our T_m models trained using molecular embeddings from mol2vec as molecular descriptors. The best results were achieved with the T_m-Tetko dataset using a deep neural network (DNN) with MAE = 31.0 K, R = 0.6 and R_{CV}^2 = 0.77. This result is already a good improvement compared to the EPI Suite with MAE = 48.6 K[29] and it is comparable to other state-of-the-art T_m regression models. As shown in Table 2, the best results have been achieved by Tetko et al.[30] using an Associative Neural Network (ASNN) and a combination of 14 classic molecular descriptors on 2078 points from the "Bradley Good Melting Point Dataset".[33] Coley et al.[35] built a T_m prediction model with MAE of 26.2 K, with very similar performances to Tetko et al. (2014) using a Convolutional Neural Network and the Attributed Molecular Graphs of 3019 chemical species from the "Bradley Good Melting Point Dataset".[31] Good results with MAE of 28.85 K were also achieved by Sivaraman et al.,[36] who developed a machine learning framework (MOLAN) for QSPR model development based on dataset specific derived embeddings and a Gaussian Process.[32] It is worth noting that the models developed in all these studies use slight variations of the "Bradley good melting point dataset" (T_m-Bradley, 3092 data points), a highly curated but very small dataset of molecules T_m (i.e., T_m-Tetko > 200 000 data points). The developed DNN model performs slightly worse than our initial expectations,
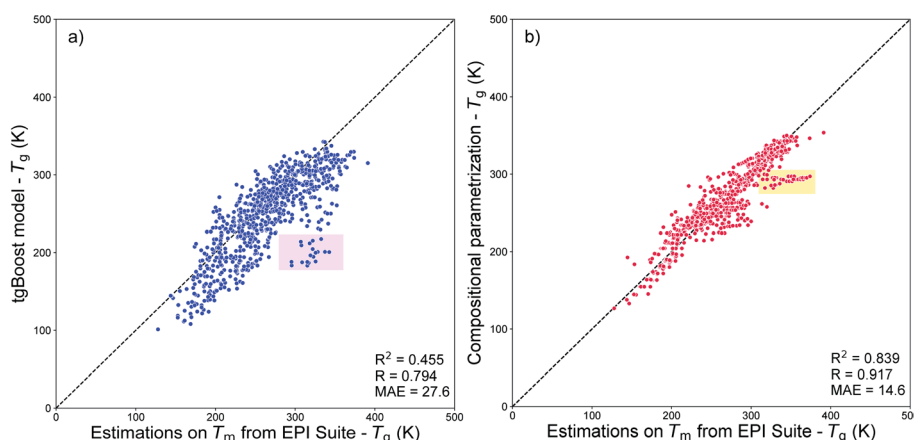

Fig. 8 (a) Correlation plot between the T_g values predicted by the tgBoost model and by the MPBPWIN module of EPI Suite for SOA compounds from Shiraiwa et al.[56] The pink squared area highlights the cluster of 20 molecules with the highest deviation between predictions. (b) Correlation plot between the T_g values predicted by the compositional parametrizations[8,15] and by the MPBPWIN module of EPI Suite for SOA compounds from Shiraiwa et al.[56] The orange squared area highlights the cluster of 30 molecules with the highest deviation between predictions.

even though the performance of machine learning models tend to refine with the increase in the amount of data used during training. A reasonable source of error might lay in the lower quality of data within the T_m-Tetko data points, which may be associated with larger experimental uncertainties compared to the T_m-Bradley dataset. Another source of error could reside in limitations of molecular embeddings and into their application to complex and large datasets. We suggest further analysis to investigate if different molecular descriptors would perform better on the T_m-Tetko dataset, but this task is beyond the scope of this study. Nevertheless, our model still performs very well in predicting T_m from their molecular structure. Remarkably, it has a lower MAE compared to T_m estimations by EPI Suite.

Molecular embeddings have already shown to be able to capture slight variations in molecular structures and physical trends for predicting T_g as discussed above. Therefore, we expect similar behavior for T_m and here we have focused our analysis on the assessment of the domain of applicability of the DNN model developed from the T_m-Tetko dataset. Fig. 9 exhibits the correlation plot between the T_m predictions from the DNN model and EPI Suite for SOA compounds from Shiraiwa et al.[56] It shows a positive correlation with $R = 0.582$, a high variance of $R_{CV}^2 = 0.261$ and a substantial divergence with MAE = 48.7 K. A deep investigation shows that the T_m of complex multi-functional species is overpredicted by EPI Suite, while the DNN model tends to overestimate the T_m of very simple compounds. The highest divergences are observed for complex multi-functional nitrate groups (EPI Suite predictions are on average 170–150 K higher than DNN ones) and for simple hydroxy acids (DNN predictions are on average 100–150 K higher than EPI Suite ones). These results suggest that our T_m model has limitations that need to be accounted if to be used to

predict the T_m of atmospheric species composing SOA. The prime cause of the discrepancy between the predictions of the two models is likely linked to the different nature of the chemical species of the datasets. Notably, the T_m-Tetko dataset has an abundance of drug-like complex compounds such as alkaloids, aromatic cyclic nitrogen bearing compounds, steroids, and polycyclic molecules as well as more molecules with Br and Cl in their structures. This chemical dissimilarity could be responsible for the low performance of the model when it tries to predict the T_m of small low functionalized organic compounds. Despite the general good performance of the DNN model on complex molecules, its application to SOA chemistry may be limited. Further investigations are needed to develop a better T_m prediction model for applications to atmospheric chemistry. Notably, future work should focus on the retrieval of a more representative dataset of experimental T_m for atmospheric species to be used for model development.

4. Conclusions

We used state-of-the-art molecular descriptors and machine learning algorithms to develop QSPR models to be used for the prediction of T_g and T_m of atmospheric organic molecules. A range of different model architectures and datasets were tested and explored for their ability to reach the best trade-off between error minimization and target prediction performance. The predictions from the developed models have been compared with available experimental data and the previously-developed T_g compositional parameterizations. Finally, the models have been tested for their applicability to SOA compounds.

The developed tgBoost model for T_g estimation is a very powerful tool: it has a low MAE of 18.3 K and its predictions are in very good agreement with experimental measurements, even capturing very subtle trends in data. The tgBoost model can reproduce non-linear trends observed in T_g for n-alkanes due to inter- and intra-molecular interactions in the bulk phase. The model can also distinguish structural isomers and discern how the positioning of a functional group within the molecular structure can influence its T_g. For this task, the tgBoost model was tested on primary, secondary and tertiary alcohols, showing how the displacement of an –OH group along the alkyl chain can influence T_g. The advantage of the tgBoost model lies in its ability to discern structural isomers; it can distinguish between aldehydes and ketones, alcohols and ethers, and esters and carboxylic acids, predicting different T_g for all pairs of isomeric chemical classes. The tgBoost model predicts the following trend in T_g sensitivity to functional group addition: –COOH (carboxylic acid) > –C(=O)OR (ester) ≈ –OH (alcohol) > –C(=O) (carbonyl) ≈ –COR (ether). This result is in good agreement with the trend in sensitivity to viscosity to functional group addition observed by Rothfuss and Petters.[16] The tgBoost model has also been tested on mono-, di- and tri-carboxylic acids in order to assess if it can capture how the interplay between multiple functional groups can affect T_g. The results are in relatively good agreement with experimental measurements, but further investigations and data are needed to refine the model for this task. Finally, the model has been tested for its
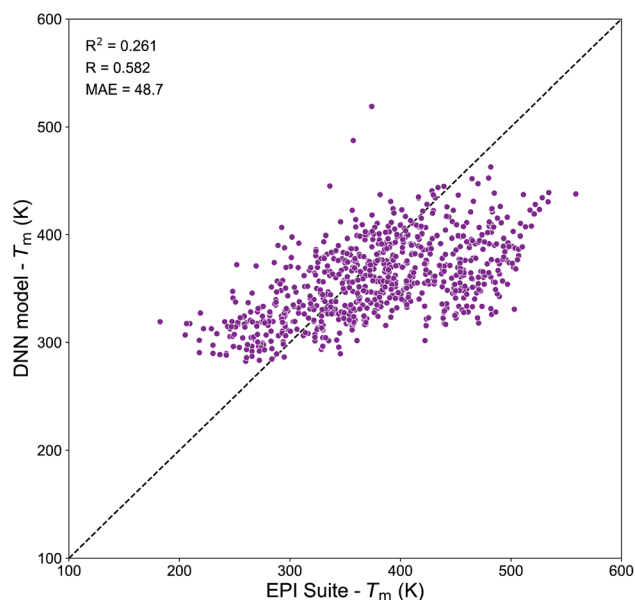

Fig. 9 Correlation plot between the T_m values predicted by the DNN model and by the MPBPWIN module of EPI Suite for SOA compounds from Shiraiwa et al.[56]

© 2022 The Author(s). Published by the Royal Society of Chemistry

Environ. Sci.: Atmos., 2022, **2**, 362–374 | **371**

applicability to SOA compounds by comparing the tgBoost model with the compositional parametrizations and EPI Suite. The tgBoost model predicts T_g in reasonable agreement with or somewhat lower compared to EPI Suite and the compositional parametrizations. This is reasonable because a major limitation of EPI Suite is known to be the overprediction of T_m of structurally complex and multi-functionalized chemical species.[29]

The DNN model developed for the prediction of the T_m of organic molecules performs well against the available dataset with MAE of 31.0 K. The model has been tested for its applicability to SOA compounds in comparison with the EPI Suite. The model performance was limited for SOA compounds, which may be due to the nature of the training dataset that is rich in drug-like complex molecules with heavy atoms within their structures. Nevertheless, the model has great potential of improvement and further studies should concentrate on the retrieval of better experimental datasets with higher fraction of atmospheric organic compounds for model training.

Considerable progress has been made with regards of the development of a T_g prediction model that includes the effects of functionality and molecular structure on T_g explicitly. This aspect is crucial for aerosol models treating gas-particle partitioning of semi-volatile compounds as strongly affected by T_g and viscosity. A difference in T_g of a few K between compositional isomers could affect the viscosity of a particle. As a result, aerosol models of complex SOA systems such as GECKO-A,[57] AIOMFAC-VISC[20] and the Master Chemical Mechanism (MCM)[58,59] would highly benefit from a more complex treatment of T_g to estimate particle viscosity. For instance, GECKO-A can generate complex chemical mechanisms formed by the reactions and partitioning between gas and particle phases. These SOA chemical systems are rich in alcohols, carboxylic acids and multi-functionalized compounds. A detailed treatment of T_g based on functionality would enhance the accuracy of model simulations and provide better insight on complex aerosol systems. The developed tgBoost model offers state-of-the-art performances in predicting the T_g of organic molecules involved in SOA chemistry. It is a very useful and powerful tool for estimations of SOA phase state and hence it can contribute to a better evaluation of SOA effects on climate and air quality.

Code availability

https://github.com/U0M0Z/tgpipe.

Conflicts of interest

There are no conflicts to declare.

Acknowledgements

References

1 J. L. Jimenez, M. R. Canagaratna, N. M. Donahue, A. S. H. Prevot, Q. Zhang, J. H. Kroll, *et al.* Evolution of organic aerosols in the atmosphere, *Science*, 2009, **326**(5959), 1525–1529.

2 U. Pöschl and M. Shiraiwa, Multiphase Chemistry at the Atmosphere-Biosphere Interface Influencing Climate and Public Health in the Anthropocene, *Chem. Rev.*, 2015, **115**(10), 4440–4475.

3 K. Tsigaridis, N. Daskalakis, M. Kanakidou, P. J. Adams, P. Artaxo, R. Bahadur, *et al.* The AeroCom evaluation and intercomparison of organic aerosol in global models, *Atmos. Chem. Phys.*, 2014, **14**(19), 10845–10895.

4 G. Ciarelli, A. Colette, S. Schucht, M. Beekmann, C. Andersson, A. Manders-Groot, *et al.* Long-term health impact assessment of total PM2.5 in Europe during the 1990–2015 period, *Atmos. Environ. X*, 2019, **3**(998), 100032, DOI: 10.1016/j.aeaoa.2019.100032.

5 M. Shrivastava, C. D. Cappa, J. Fan, A. H. Goldstein, A. B. Guenther, J. L. Jimenez, *et al.* Recent advances in understanding secondary organic aerosol: Implications for global climate forcing, *Rev. Geophys.*, 2017, **55**(2), 509–559.

6 Y. Li and M. Shiraiwa, Timescales of secondary organic aerosols to reach equilibrium at various temperatures and relative humidities, *Atmos. Chem. Phys.*, 2019 May 7, **19**(9), 5959–5971.

7 T. Koop, J. Bookhold, M. Shiraiwa and U. Pöschl, Glass transition and phase state of organic compounds: Dependency on molecular properties and implications for secondary organic aerosols in the atmosphere, *Phys. Chem. Chem. Phys.*, 2011, **13**(43), 19238–19255.

8 W. S. W. DeRieux, Y. Li, P. Lin, J. Laskin, A. Laskin, A. K. Bertram, *et al.* Predicting the glass transition temperature and viscosity of secondary organic material using molecular composition, *Atmos. Chem. Phys.*, 2018, **18**(9), 6331–6351.

9 T. Galeazzo, R. Valorso, Y. Li, M. Camredon, B. Aumont and M. Shiraiwa, Estimation of Secondary Organic Aerosol Viscosity from Explicit Modeling of Gas-Phase Oxidation of Isoprene and α-pinene, *Atmos. Chem. Phys.*, 2021, 1–23.

10 H. P. Dette, M. Qi, D. C. Schröder, A. Godt and T. Koop, Glass-forming properties of 3-methylbutane-1,2,3-tricarboxylic acid and its mixtures with water and pinonic acid, *J. Phys. Chem. A*, 2014, **118**(34), 7024–7033.

11 S. S. Petters, S. M. Kreidenweis, A. P. Grieshop, P. J. Ziemann and M. D. Petters, Temperature- and Humidity-Dependent Phase States of Secondary Organic Aerosols, *Geophys Res. Lett.*, 2019, **46**(2), 1005–1013.

12 Y. Zhang, L. Nichman, P. Spencer, J. I. Jung, A. Lee, B. K. Heffernan, *et al.* The Cooling Rate- And Volatility-Dependent Glass-Forming Properties of Organic Aerosols Measured by Broadband Dielectric Spectroscopy, *Environ. Sci. Technol.*, 2019, **53**(21), 12366–12378.

13 M. Shiraiwa, Y. Li, A. P. Tsimpidi, V. A. Karydis, T. Berkemeier, S. N. Pandis, *et al.* Global distribution of

particle phase state in atmospheric secondary organic aerosols, *Nat. Commun.*, 2017, **8**(1), 15002.

14 N. E. Rothfuss and M. D. Petters, Influence of Functional Groups on the Viscosity of Organic Aerosol, *Environ. Sci. Technol.*, 2017, **51**(1), 271–279.

15 Y. Li, D. A. Day, H. Stark, J. L. Jimenez and M. Shiraiwa, Predictions of the glass transition temperature and viscosity of organic aerosols from volatility distributions, *Atmos. Chem. Phys.*, 2020, **20**(13), 8103–8122.

16 N. E. Rothfuss and M. D. Petters, Influence of Functional Groups on the Viscosity of Organic Aerosol, *Environ. Sci. Technol.*, 2017, **51**(1), 271–279.

17 S. K. Schum, B. Zhang, K. Dzepina, P. Fialho, C. Mazzoleni and L. R. Mazzoleni, Molecular and physical characteristics of aerosol at a remote free troposphere site: Implications for atmospheric aging, *Atmos. Chem. Phys.*, 2018, **18**(19), 14017–14036.

18 J. C. Ditto, T. Joo, P. Khare, R. Sheu, M. Takeuchi, Y. Chen, *et al.* Effects of Molecular-Level Compositional Variability in Organic Aerosol on Phase State and Thermodynamic Mixing Behavior, *Environ. Sci. Technol.*, 2019, **53**(22), 13009–13018. Available from: https://pubs.acs.org/doi/abs/10.1021/acs.est.9b02664.

19 M. Song, A. M. MacLean, Y. Huang, N. R. Smith, S. L. Blair, J. Laskin, *et al.* Liquid-liquid phase separation and viscosity within secondary organic aerosol generated from diesel fuel vapors, *Atmos. Chem. Phys.*, 2019, **19**(19), 12515–12529.

20 N. R. Gervasi, D. O. Topping and A. Zuend, A predictive group-contribution model for the viscosity of aqueous organic aerosol, *Atmos. Chem. Phys.*, 2020, **20**(5), 2987–3008.

21 M. Octaviani, M. Shrivastava, R. A. Zaveri, A. Zelenyuk, Y. Zhang, Q. Z. Rasool, *et al.* Modeling the Size Distribution and Chemical Composition of Secondary Organic Aerosols during the Reactive Uptake of Isoprene-Derived Epoxydiols under Low-Humidity Condition, *ACS Earth Sp Chem*, 2021, **5**(11), 3247–3257.

22 R. Schmedding, M. Ma, Y. Zhang, S. Farrell, H. O. T. Pye, Y. Chen, *et al.* A-Pinene-Derived organic coatings on acidic sulfate aerosol impacts secondary organic aerosol formation from isoprene in a box model, *Atmos. Environ.*, 2019, **213**(June), 456–462, DOI: 10.1016/j.atmosenv.2019.06.005.

23 R. Schmedding, Q. Z. Rasool, Y. Zhang, H. O. T. Pye, H. Zhang, Y. Chen, *et al.* Predicting secondary organic aerosol phase state and viscosity and its effect on multiphase chemistry in a regional-scale air quality model, *Atmos. Chem. Phys.*, 2020, **20**(13), 8201–8225.

24 R. Todeschini and V. Consonni. *Molecular Descriptors for Chemoinformatics Volume I: Alphabetical Listing/Volume II: Append*. 2nd edn, Weinheim, Wiley-VCH, 2009.

25 H. van de Waterbeemd and E. Gifford, ADMET in silico modelling: towards prediction paradise?, *Nat. Rev. Drug Discovery*, 2003, **2**(3), 192–204. Available from: http://www.nature.com/articles/nrd1032.

26 Y. Ran, N. Jain and S. H. Yalkowsky, Prediction of Aqueous Solubility of Organic Compounds by the General Solubility Equation (GSE), *J. Chem. Inf. Comput. Sci.*, 2001, **41**(5),

1208–1217. Available from: https://pubs.acs.org/doi/10.1021/ci010287z.

27 J. Nikmo, J. Kukkonen and K. Riikonen, A model for evaluating physico-chemical substance properties required by consequence analysis models, *J. Hazard. Mater.*, 2002, **91**(1–3), 43–61. Available from: https://linkinghub.elsevier.com/retrieve/pii/S030438940100379X.

28 U. P. Preiss, W. Beichel, A. M. T. Erle, Y. U. Paulechka and I. Krossing, Is Universal, Simple Melting Point Prediction Possible?, *ChemPhysChem*, 2011, **12**(16), 2959–2972. Available from: https://onlinelibrary.wiley.com/doi/10.1002/cphc.201100522.

29 EPA U. *Estimation Programs Interface SuiteTM for Microsoft Windows v4.1.1*. Washington, DC, USA: United States Environmental Protection Agency; 2017.

30 S. Jastrzębski, D. Leśniak, W. M. Czarnecki. *Learning to SMILE(S)*. 2016;1–5. Available from: http://arxiv.org/abs/1602.06289.

31 R. Gómez-Bombarelli, J. N. Wei, D. Duvenaud, J. M. Hernández-Lobato, B. Sánchez-Lengeling, D. Sheberla, *et al.* Automatic Chemical Design Using a Data-Driven Continuous Representation of Molecules, *ACS Cent. Sci.*, 2018, **4**(2), 268–276.

32 M. H. S. Segler, T. Kogej, C. Tyrchan and M. P. Waller, Generating focused molecule libraries for drug discovery with recurrent neural networks, *ACS Cent. Sci.*, 2018, **4**(1), 120–131.

33 S. Jaeger, S. Fulle and S. Turk, Mol2vec: Unsupervised Machine Learning Approach with Chemical Intuition, *J. Chem. Inf. Model*, 2018, **58**(1), 27–35.

34 I. V. Tetko, Y. Sushko, S. Novotarskyi, L. Patiny, I. Kondratov, A. E. Petrenko, *et al.* How accurately can we predict the melting points of drug-like compounds?, *J. Chem. Inf. Model*, 2014, **54**(12), 3320–3329.

35 C. W. Coley, R. Barzilay, W. H. Green, T. S. Jaakkola and K. F. Jensen, Convolutional Embedding of Attributed Molecular Graphs for Physical Property Prediction, *J. Chem. Inf. Model*, 2017, **57**(8), 1757–1772.

36 G. Sivaraman, N. E. Jackson, B. Sanchez-Lengeling, Vázquez-Mayagoitia Á, A. Aspuru-Guzik, V. Vishwanath, *et al.* A machine learning workflow for molecular analysis: application to melting points, *Mach Learn Sci Technol*, 2020, **1**(2), 025015.

37 *RDKit.03.1*, 2021, Open-source cheminformatics.

38 M. Martín-Betancourt, J. M. Romero-Enrique and L. F. Rull, Molecular simulation study of the glass transition for a flexible model of linear alkanes, *Mol. Simul.*, 2009, **35**(12–13), 1043–1050.

39 I. V. Tetko, M. Lowe D and A. J. Williams, The development of models to predict melting and pyrolysis point data associated with several hundred thousand compounds mined from PATENTS, *J. Cheminform.*, 2016, **8**(1), 1–18.

40 J.-C. Bradley, A. Lang and A. J. Williams, *Jean-Claude Bradley Double Plus Good (Highly Curated and Validated) Melting Point Dataset*, 2014.

© 2022 The Author(s). Published by the Royal Society of Chemistry

Environ. Sci.: Atmos., 2022, **2**, 362–374 | **373**

41 T. Chen, C. Guestrin. XGBoost: A Scalable Tree Boosting System, in *22nd SIGKDD Conference on Knowledge Discovery and Data Mining*. 2016.

42 G. Varoquaux, P. R. Raamana, D. A. Engemann, A. Hoyos-Idrobo, Y. Schwartz and B. Thirion, Assessing and tuning brain decoders: Cross-validation, caveats, and guidelines, *Neuroimage*, 2017, **145**, 166–179.

43 D. Krstajic, L. J. Buturovic, D. E. Leahy and S. Thomas, Cross-validation pitfalls when selecting and assessing regression and classification models, *J. Cheminform.*, 2014 Dec 29, **6**(1), 10. Available from: **https://jcheminf.biomedcentral.com/articles/10.1186/1758-2946-6-10**.

44 G. C. Cawley and N. L. C. Talbot, On over-fitting in model selection and subsequent selection bias in performance evaluation, *J. Mach. Learn. Res.*, 2010, **11**, 2079–2107.

45 F. Pedregosa, G. Varoquaux, A. Gramfort, V. Michel, B. Thirion, O. Grisel, *et al.* Scikit-learn: Machine Learning in Python, *J. Mach. Learn. Res.*, 2011, **12**, 2825–2830. Available from: **https://jmlr.org/papers/volume12/pedregosa11a/pedregosa11a.pdf**.

46 T. Hastie, R. Tibshirani and J. H. Friedman. *The Elements of Statistical Learning: Data Mining, Inference, and Prediction*. 2nd edn New York, NY, USA, Springer, 2009, p. 745.

47 F. Chollet, *Keras Github*, 2015, **https://github.com/fchollet/keras**.

48 J. D. Surratt, A. W. H. Chan, N. C. Eddingsaas, M. N. Chan, C. L. Loza, A. J. Kwan, *et al.* Reactive intermediates revealed in secondary organic aerosol formation from isoprene, *Proc. Natl. Acad. Sci. U. S. A.*, 2010, **107**(15), 6640–6645.

49 H. Zhang, J. D. Surratt, Y. H. Lin, J. Bapat and R. M. Kamens, Effect of relative humidity on SOA formation from isoprene/NO photooxidation: Enhancement of 2-methylglyceric acid and its corresponding oligoesters under dry conditions, *Atmos. Chem. Phys.*, 2011, **11**(13), 6411–6424.

50 P. J. Ziemann and R. Atkinson, Kinetics, products, and mechanisms of secondary organic aerosol formation, *Chem. Soc. Rev.*, 2012, **41**(19), 6582–6605.

51 M. C. Etter, Encoding and Decoding Hydrogen-Bond Patterns of Organic Compounds, *Acc. Chem. Res.*, 1990, **23**(4), 120–126.

52 T. L. McConnell, C. A. Wheaton, K. C. Hunter and S. D. Wetmore, Effects of Hydrogen Bonding on the Acidity of Adenine, Guanine, and Their 8-Oxo Derivatives, *J. Phys.*

Chem. A, 2005 Jul 1, **109**(28), 6351–6362. Available from: **https://pubs.acs.org/doi/10.1021/jp0509919**.

53 J. Graton, F. Besseau, A. M. Brossard, E. Charpentier, A. Deroche and J. Y. Le Questel, Hydrogen-bond acidity of OH groups in various molecular environments (phenols, alcohols, steroid derivatives, and amino acids structures): Experimental measurements and density functional theory calculations, *J. Phys. Chem. A*, 2013, **117**(49), 13184–13193.

54 A. Laventure, A. Gujral, O. Lebel, C. Pellerin and M. D. Ediger, Influence of Hydrogen Bonding on the Kinetic Stability of Vapor-Deposited Glasses of Triazine Derivatives, *J. Phys. Chem. B*, 2017, **121**(10), 2350–2358.

55 A. Laventure, G. De Grandpré, A. Soldera, O. Lebel and C. Pellerin, Unraveling the interplay between hydrogen bonding and rotational energy barrier to fine-tune the properties of triazine molecular glasses, *Phys. Chem. Chem. Phys.*, 2016, **18**(3), 1681–1692.

56 M. Shiraiwa, T. Berkemeier, K. A. Schilling-Fahnestock, J. H. Seinfeld and U. Pöschl, Molecular corridors and kinetic regimes in the multiphase chemical evolution of secondary organic aerosol, *Atmos. Chem. Phys.*, 2014, **14**(16), 8323–8341.

57 B. Aumont, S. Szopa and S. Madronich, Modelling the evolution of organic carbon during its gas-phase tropospheric oxidation: development of an explicit model based on a self generating approach, *Atmos. Chem. Phys.*, 2005, **5**(1), 703–754.

58 M. E. Jenkin, S. M. Saunders, V. Wagner and M. J. Pilling, Protocol for the development of the Master Chemical Mechanism, MCM v3 (Part B): Tropospheric degradation of aromatic volatile organic compounds, *Atmos. Chem. Phys.*, 2003, **3**(1), 181–193.

59 M. E. Jenkin, J. C. Young and A. R. Rickard, The MCM v3.3.1 degradation scheme for isoprene, *Atmos. Chem. Phys.*, 2015, **15**(20), 11433–11459.

60 D. K. Duvenaud, D. Maclaurin, J. Aguilera-Iparraguirre, R. Gomez-Bombarelli, T. Hirzel, A. Aspuru-Guzik and R. P. Adams, Convolutional Networks on Graphs for Learning Molecular Fingerprints, *Adv. Neural Inf. Process. Syst.*, 2015, 2215–2223, **https://doi.org/10.48550/arXiv.1509.09292**.

61 S. Kearnes, K. McCloskey, M. Berndl, V. Pande and P. Riley, Molecular Graph Convolutions: Moving Beyond Fingerprints, *J. Comput.-Aided Mol. Des.*, 2016, **30**, 595–608, **https://doi.org/10.1007/s10822-016-9938-8**.